Eur. Phys. J. D **36**, 143–157 (2005)
DOI: 10.1140/epjd/e2005-00217-3

THE EUROPEAN PHYSICAL JOURNAL D

Microscopic theory of optical excitations, photoluminescence, and terahertz response in semiconductors

M. Kira and S.W. Koch[a]

Fachbereich Physik und Wissenschaftliches Zentrum für Materialwissenschaften, Philipps Universität, Renthof 5, 35032 Marburg, Germany

Received 15 April 2005 / Received in final form 9 June 2005
Published online 9 August 2005 –

Abstract. This article presents a comprehensive many-body theory for optically excited semiconductors. The coupled equations of motion for the correlation functions of the Coulomb-interacting electron-hole system are derived and solved for different excitation conditions. The generation of a coherent excitonic polarization and its conversion into incoherent populations is analyzed. The spontaneous emission properties of the excited system are evaluated using a fully quantized theory. Luminescence from excitonic and electron-hole plasma populations is computed, and significant hole burning in the exciton center of mass distributions is predicted. It is shown how different excitations states of the many-body system can be identified by their characteristic signatures in the absorption spectra of a terahertz probe field.

PACS. 71.35.-y Excitons and related phenomena – 42.50.-p Quantum optics – 78.47.+p Time-resolved optical spectroscopies and other ultrafast optical measurements in condensed matter

1 Introduction

Optically excited electrons and holes in a semiconductor establish a Coulomb interacting many-body Fermion system which exhibits characteristic dynamical features that occur on a wide range of different time scales [1,2]. Resonant excitation of the semiconductor induces an interband polarization which is subject to various interaction processes leading to dephasing and/or conversion into incoherent populations. Besides dynamical rearrangements and reconfigurations in their respective quantum states, these populations can also decay radiatively by spontaneously emitting photons.

In order to microscopically model these effects, we have to deal not only with the Coulomb interacting many-body system of electron-hole excitations but also with their coupling to the classical and/or quantized light field. For this purpose, we use density-matrix theory to derive equations of motion for the coupled carrier-photon-phonon system. We consistently truncate the resulting hierarchies of the relevant expectation values and compute photonic correlation functions which are directly accessible in experiments.

The theory is applied to investigate the conditions under which a truly incoherent excitonic population forms and how it could be identified experimentally. Excitonic features in linear absorption spectra are clearly not related to any population effect since only the induced optical polarization and no population exists in the linear regime. The presence of some form of an electron-hole-pair population is required to observe photoluminescence (PL) under incoherent conditions. However, our calculations show that the mere appearance of excitonic resonances in PL spectra is not sufficient to draw conclusions about the presence of excitons since also unbound electron-hole pairs can give rise to these features [3].

As an unambiguous method to identify excitonic populations, we investigate terahertz (THz) spectroscopy which can be used to probe transitions between excitonic eigenstates [4–7] and other effects [8–11] in many-body systems. Under incoherent conditions, the observation of resonances due to these transitions is a clear signature of an exciton population. The resonances in the THz absorption correspond to differences between energy eigenvalues related to the relative electron-hole motion. They are independent of the exciton's center-of-mass energy as long as momentum dependent energy renormalizations are negligible. Therefore, the induced THz absorption is basically insensitive to the exciton-distribution function.

This article presents an overview and a summary of our many-body cluster-expansion approach. We start in Section 2 with a presentations of the basic Hamiltonian for the interacting electron-hole-photon-phonon system. Then we summarize the equation of motion approach and the consistent cluster-expansion scheme. Concentrating on the semiclassical regime, we derive in Section 3 the general semiconductor Bloch equations. We present examples of their solutions for special cases, as well as the nonlinear optical response related to the effect of excitation induced

[a] e-mail: stephan.w.koch@physik.uni-marburg.de

dephasing due to the many-body Coulomb interaction. In Section 4 we then analyze the conversion of a coherent polarization into incoherent populations. The spontaneous emission from semiconductors is discussed in Section 5, and in Section 6 we study the linear THz-response of a Coulomb interacting electron-hole system. In all cases, we pay attention to excitonic features and their microscopic origin.

2 Consistent many-body theory

In this section, we outline the microscopic treatment of a semiconductor many-body system which is coupled to the quantized light field and lattice vibrations. Since different aspects this general problem have been discussed thoroughly in the literature [1,12,13], we just briefly summarize the fundamental properties relevant for this paper.

The optically active electrons in their Bloch bands are described with the help of the fermionic operators $a^\dagger_{\mathbf{k},\lambda}$ and $a_{\mathbf{k},\lambda}$ where, e.g., $a_{\mathbf{k},\lambda}$ annihilates an electron with momentum $\mathbf{k}$ and λ is the combined band and spin index. In many experimentally relevant situations, the carrier dynamics takes place between one conduction band ($\lambda = c$) and one valence band ($\lambda = v$) such that we restrict the analysis to such two-band systems.

For a quantum mechanical description of the transverse electro-magnetic field, we start from the vector potential $\mathbf{A}$ within the canonical quantization scheme [12]. The vector potential can be expanded in terms of the steady-state mode functions $\mathbf{U}_{\mathbf{q}\sigma}(\mathbf{r})$ where $\mathbf{q}$ is the wave vector and σ is the polarization index. By using a complete basis of mode functions, the operator $\mathbf{A}$ can be expressed in terms of creation and annihilation operators of photons corresponding to each eigenmode,

$$\mathbf{A}(\mathbf{r},z) = \sum_{\mathbf{q},q_z} \mathcal{E}_\mathbf{q}/\omega_\mathbf{q} \left[\mathbf{U}_\mathbf{q}(\mathbf{r}) B_\mathbf{q} + \text{h.c.}\right] \tag{1}$$

where $\mathcal{E}_\mathbf{q} = \sqrt{\hbar\omega_\mathbf{q}/(2\epsilon_0)}$ is the so-called vacuum field amplitude, $\omega_\mathbf{q} = c|\mathbf{q}|$ is the optical frequency, and $B_\mathbf{q}$ is the bosonic photon destruction operator. The quantized lattice vibrations can be treated similarly introducing the bosonic operators $D_\mathbf{p}$ and $D^\dagger_\mathbf{p}$ for phonons with momentum $\mathbf{p}$.

The total system Hamiltonian,

$$H_{tot} = H_0 + H_C + H_D + H_P, \tag{2}$$

consists of the non-interacting contribution H_0, the Coulomb interaction among the carriers H_C, the light-carrier interaction H_D, and the carrier-phonon interaction H_P. To elaborate the details in H_{tot}, we start from

$$H_0 = \sum_\mathbf{k} \left[\epsilon^c_\mathbf{k} a^\dagger_{c,\mathbf{k}} a_{c,\mathbf{k}} + \epsilon^v_\mathbf{k} a^\dagger_{v,\mathbf{k}} a_{v,\mathbf{k}}\right] + \sum_\mathbf{q} \hbar\omega_\mathbf{q} \left(B^\dagger_\mathbf{q} B_\mathbf{q} + \frac{1}{2}\right) + \sum_\mathbf{p} \hbar\Omega_\mathbf{p} \left(D^\dagger_\mathbf{p} D_\mathbf{p} + \frac{1}{2}\right), \tag{3}$$

which contains the non-interacting carriers, photons, and phonons, respectively. The corresponding carrier energies are

$$\epsilon^c_\mathbf{k} = \frac{\hbar^2\mathbf{k}^2}{2m_e} + E_g, \tag{4}$$

$$\epsilon^v_\mathbf{k} = -\frac{\hbar^2\mathbf{k}^2}{2m_h}, \tag{5}$$

with the band-gap energy E_g and the reduced electron and hole masses $m_{e,h}$. The phonon dispersion is given by $\Omega_\mathbf{p}$.

The Coulombic many-body Hamiltonian of the carriers is

$$H_C = \frac{1}{2} \sum_{\mathbf{k},\mathbf{k}',\mathbf{q}\neq\mathbf{0}} V_\mathbf{q} [a^\dagger_{c,\mathbf{k}+\mathbf{q}} a^\dagger_{c,\mathbf{k}'-\mathbf{q}} a_{c,\mathbf{k}'} a_{c,\mathbf{k}} + a^\dagger_{v,\mathbf{k}+\mathbf{q}} a^\dagger_{v,\mathbf{k}'-\mathbf{q},} a_{v,\mathbf{k}'} a_{v,\mathbf{k}} + 2a^\dagger_{c,\mathbf{k}+\mathbf{q}} a^\dagger_{v,\mathbf{k}'-\mathbf{q}} a_{v,\mathbf{k}'} a_{c,\mathbf{k}}] \tag{6}$$

with the bare Coulomb matrix element $V_\mathbf{k}$ [14]. The interaction between the optical photons and carriers follows from

$$H_D = -\sum_{\mathbf{q},\mathbf{k}} i\mathcal{F}_\mathbf{q} \left(a^\dagger_{v,\mathbf{k}} a_{c,\mathbf{k}-\mathbf{q}} + a^\dagger_{c,\mathbf{k}} a_{v,\mathbf{k}-\mathbf{q}}\right) B_\mathbf{q} + \text{h.c.}, \tag{7}$$

with $\mathcal{F}_\mathbf{q} \equiv d_{v,c} U_\mathbf{q} \mathcal{E}_\mathbf{q}$ where $d_{v,c}$ is the dipole-matrix element. Finally, the phonon-carrier interaction is given by

$$H_\text{P} = \sum_{\mathbf{p},\mathbf{k}} [G^c_p (D_\mathbf{p} + D^\dagger_{-\mathbf{p}}) a^\dagger_{c,\mathbf{k}} a_{c,\mathbf{k}-\mathbf{p}} + G^v_\mathbf{p} (D_\mathbf{p} + D^\dagger_{-\mathbf{p}}) a^\dagger_{v,\mathbf{k}} a_{v,\mathbf{k}-\mathbf{p}}]. \tag{8}$$

The strength of the phonon-carrier interaction is determined by the form factor $G^\lambda_\mathbf{p}$ [15].

2.1 Equations of motion and hierarchy problem

In general, the system properties can always be traced back to quantum mechanical operators O and their expectation values $\langle O\rangle = \text{Tr}\,[O\rho]$ where ρ is the statistical operator of the system. In the following, we apply the Heisenberg equation of motion $i\hbar\frac{\partial}{\partial t}O = [O, H_{tot}]$ to derive the quantum dynamics for the interacting carrier-photon-phonon system of the semiconductor. To classify the physically relevant operators, we note, that

$$O_N = a^\dagger_1 ... a^\dagger_N a_N ... a_1, \tag{9}$$

always corresponds to an N-particle operator. Here, we use the notation that the index $j = (\lambda_j, \mathbf{k}_j)$ contains the band and momentum index of the corresponding operator. From a purely formal point of view, a single photon and phonon operator correspond to a single-particle operator. Thus, a general N-particle operator has the form

$$O_N = B^\dagger_1 ... B^\dagger_{N_1} D^\dagger_1 ... D^\dagger_{N_2} a^\dagger_1 ... a^\dagger_{N_3} a_{N_3} ... a_1 D_{N_4} ... D_1 B_{N_5} ... B_1, \tag{10}$$

with all possible combinations of N_j fulfilling $N_1 + N_2 + N_3 + N_4 + N_5 = N$. According to this classification, H_C, H_P, and H_D, correspond to two-particle interactions.

When the Heisenberg equations of motion are derived, we notice that single-particle operators couple to two-particle operators due to the Coulomb, light-matter, and phonon-matter interactions. This coupling leads to an infinite hierarchy of operator equations, where all orders and mixtures of operators are present. Since the equations of motion for expectation values are directly obtained from those of the operators, they inherit the same hierarchy problem,

$$i\frac{\partial}{\partial t}\langle N\rangle = T[\langle N\rangle] + V[\langle N+1\rangle], \tag{11}$$

where the N-particle expectation value $\langle N\rangle$ couples to higher order $\langle N+1\rangle$ quantities via the functional V. The functional T results mainly from the noninteracting part of the Hamiltonian while V originates from the interactions. Since equation (11) cannot be closed, we will used a systematic truncation scheme to obtain controlled approximations for the Coulomb correlations, the semiclassical, and the quantum optical effects in solids.

2.2 Consistent truncation of correlation hierarchy

One successful approach to deal with the hierarchy problem is to use the so-called cluster-expansion [5,16–18]. This method is based on a scheme where one determines all consistent factorizations of an N-particle quantity $\langle N\rangle$ in terms of (i) independent single particles (singlets); (ii) correlated pairs (doublets); (iii) correlated three-particle clusters (triplets); up to (iv) correlated N-particle clusters. A systematic treatment of the hierarchy problem is obtained if one truncates the right-hand side of equation (11) such that one includes all clusters up to a given level.

In practice, the cluster-expansion scheme can be determined recursively if we assume that we formally know all expectation values from $\langle 1\rangle$ to $\langle N\rangle$. A specific correlated cluster then follows recursively via

$$\langle 2\rangle = \langle 2\rangle_{\rm S} + \Delta\langle 2\rangle \tag{12}$$

$$\langle 3\rangle = \langle 3\rangle_{\rm S} + \langle 1\rangle\Delta\langle 2\rangle + \Delta\langle 3\rangle \tag{13}$$

$$\langle N\rangle = \langle N\rangle_{\rm S} + \langle N-2\rangle_{\rm S}\Delta\langle 2\rangle + \langle N-4\rangle_{\rm S}\Delta\langle 2\rangle\Delta\langle 2\rangle + ... + \Delta\langle N\rangle. \tag{14}$$

Here, the quantities $\Delta\langle N\rangle$ contain the purely correlated part of the N-particle cluster. In equations (12–14), each term denotes a sum over all possibilities to reorganize the N coordinates among singlets, doublets, and so on by including the possible sign changes due to the permutations of the carrier operators. This way all cluster groups in equation (14) are fully antisymmetric for fermionic carriers and symmetric for bosonic photon and phonon operators.

After the identification of the individual clusters, one can easily introduce a consistent truncation, such as

$$\langle N\rangle_{\rm S} = \langle N\rangle_{\rm HF}, \tag{15}$$

$$\langle N\rangle_{\rm D} = \langle N-2\rangle_{\rm S}\Delta\langle 2\rangle + \langle N-4\rangle_{\rm S}\Delta\langle 2\rangle\Delta\langle 2\rangle + ..., \tag{16}$$

for singlets or doublets, respectively. In practice, $\langle N\rangle_{\rm S}$ is given by the Hartree-Fock approximation with all possible combinations containing only single-particle expectation values. The doublet part follows from all expectation values with one or more correlated pairs $\Delta\langle 2\rangle$ combined with the corresponding contribution of singlets $\langle 1\rangle$.

If we only include plasma and exciton effects in our analysis, an arbitrary N-particle expectation value can be expressed consistently at the level of the singlet-doublet approximation,

$$\langle N\rangle_{\rm SD} = \langle N\rangle_{\rm S} + \langle N\rangle_{\rm D}. \tag{17}$$

This determines uniquely how the truncation of the hierarchy has to be performed; we only need to solve the dynamics of $\langle 1\rangle$ and $\Delta\langle 2\rangle$ because any arbitrary $\langle N\rangle_{\rm SD}$ consist only of the two-point expectation values and four-point correlations. According to equation (11), we obtain

$$i\hbar\frac{\partial}{\partial t}\langle 1\rangle = T_1[\langle 1\rangle] + V_1[\langle 2\rangle_{\rm S}] + V_1[\Delta\langle 2\rangle], \tag{18}$$

$$i\hbar\frac{\partial}{\partial t}\Delta\langle 2\rangle = T_2[\Delta\langle 2\rangle] + V_2[\langle 3\rangle_{\rm SD}], \tag{19}$$

where $T_{1(2)}$ and $V_{1(2)}$ are known functionals defined by the specific form of the Heisenberg equation of motion. The consistent singlet-doublet approximation is obtained when $\langle 3\rangle$ is approximated by $\langle 3\rangle_{\rm SD}$. As a result, the infinite hierarchy is systematically truncated and the set of equations (18) and (19) is closed.

3 Semiconductor bloch equations

The classical part of the light field results directly from the coherent amplitudes $\langle B_q\rangle$ and $\langle B_q^\dagger\rangle$ such that only the electric field,

$$\langle E(\mathbf{r},t)\rangle = \sum_{\mathbf{q}}\left[i\mathcal{E}_{\mathbf{q}}\mathbf{U}_{\mathbf{q}}(\mathbf{r})\langle B_{\mathbf{q}}\rangle - i\mathcal{E}_{\mathbf{q}}\mathbf{U}^\star_{\mathbf{q}}(\mathbf{r})\langle B^\dagger_{\mathbf{q}}\rangle\right], \tag{20}$$

is needed. To illustrate the basic features of light-matter interaction at the semi-classical level, we first concentrate on the excitations generated by such classical fields.

The Heisenberg equation of motion for $\langle E\rangle$ yields the well-known wave equation

$$\left[\nabla^2 - \frac{n^2(z)}{c^2}\frac{\partial^2}{\partial t^2}\right]\langle E(z,t)\rangle = \mu_0\frac{\partial^2}{\partial t^2}P(z), \tag{21}$$

where we have assume light field propagation in the z-direction perpendicular to a planar structure with background refractive index $n(z)$. The semiconductor system is assumed to be either a quantum well (QW) or a planar

arrangement of quantum wires such that the polarization, $P(z)$, has only a spatial z dependency.

To determine $P(z)$, we have to investigate the specific excitation of the planar semiconductor structure. If we assume strongly confined quantum wells or wires, the z-dependence of $P(z)$ results only from the confinement function $g(z)$. Hence, the only real task is to compute the amplitude of the macroscopic polarization. Using a Bloch expansion, we can write the macroscopic polarization as $P = (1/\mathcal{L}^d)\sum_k d_{vc}P_{\mathbf{k}} + \text{c.c}$ with the dipole-matrix element d_{vc} and normalization volume $\mathcal{L}^d$. Here, $P_{\mathbf{k}}$ is the microscopic polarization $P_{\mathbf{k}} \equiv \langle a^\dagger_{\mathbf{k},v} a_{\mathbf{k},c}\rangle$ of our two-band system with one conduction (subscript c) and one valence (subscript v) band; $P_{\mathbf{k}}$ is also coupled to the occupation probabilities of electrons $f^e_{\mathbf{k}} \equiv \langle a^\dagger_{\mathbf{k},c} a_{\mathbf{k},c}\rangle$, and holes $f^h_{\mathbf{k}} \equiv \langle a_{\mathbf{k},v} a^\dagger_{\mathbf{k},v}\rangle$.

From the Heisenberg equations of motion for the individual operators, we obtain

$$i\hbar\frac{\partial}{\partial t}P_{\mathbf{k}} = \tilde{\epsilon}_{\mathbf{k}}P_{\mathbf{k}} - \left[1 - f^e_{\mathbf{k}} - f^h_{\mathbf{k}}\right]\Omega_{\mathbf{k}} - i\Gamma_{\mathbf{k}}, \tag{22}$$

$$\frac{\hbar}{2}\frac{\partial}{\partial t}f^e_{\mathbf{k}} = \mathrm{Im}\left[P_{\mathbf{k}}\Omega^\star_{\mathbf{k}} + \sum_{\mathbf{q},\mathbf{k}',\lambda} V_{\mathbf{q}} c^{\mathbf{q},\mathbf{k}',\mathbf{k}}_{c,\lambda,\lambda,c} + \sum_{\mathbf{q}} \mathcal{D}^{\mathrm{c,c}}_{\mathbf{k},\mathbf{q}}\right], \tag{23}$$

$$\frac{\hbar}{2}\frac{\partial}{\partial t}f^h_{\mathbf{k}} = \mathrm{Im}\left[P_{\mathbf{k}}\Omega^\star_{\mathbf{k}} - \sum_{\mathbf{q},\mathbf{k}',\lambda} V_{\mathbf{q}} c^{\mathbf{q},\mathbf{k}',\mathbf{k}}_{v,\lambda,\lambda,v} - \sum_{\mathbf{q}} \mathcal{D}^{\mathrm{v,v}}_{\mathbf{k},\mathbf{q}}\right], \tag{24}$$

with the renormalized kinetic electron-hole-pair energy

$$\tilde{\epsilon}_{\mathbf{k}} \equiv \epsilon^c_{\mathbf{k}} - \epsilon^v_{\mathbf{k}} - \sum_{\mathbf{k}'} V_{\mathbf{k}-\mathbf{k}'}\left(f^e_{\mathbf{k}'} + f^h_{\mathbf{k}'}\right), \tag{25}$$

and the renormalized Rabi frequency

$$\Omega_{\mathbf{k}} \equiv d_{cv}E(0,t) + \sum_{\mathbf{k}'} V_{\mathbf{k}-\mathbf{k}'}P_{\mathbf{k}'}. \tag{26}$$

The last term of equation (22) contains the correlated two-particle contributions

$$i\Gamma_{\mathbf{k}} = \sum_{\mathbf{q}}\left[V_{\mathbf{q}}\sum_{\mathbf{n},\lambda} c^{\mathbf{q},\mathbf{n},\mathbf{k}}_{v,\lambda,\lambda,c} - \mathcal{D}^{\mathrm{v,c}}_{\mathbf{k},\mathbf{q}}\right] - [c \leftrightarrow v]^\star. \tag{27}$$

Here, the true two-particle correlations are defined as

$$\begin{aligned} c^{\mathbf{q},\mathbf{k}',\mathbf{k}}_{\lambda,\nu,\nu',\lambda'} &\equiv \Delta\langle a^\dagger_{\lambda,\mathbf{k}} a^\dagger_{\nu,\mathbf{k}'} a_{\nu',\mathbf{k}'+\mathbf{q}} a_{\lambda',\mathbf{k}-\mathbf{q}}\rangle \\ &= \langle a^\dagger_{\lambda,\mathbf{k}} a^\dagger_{\nu,\mathbf{k}'} a_{\nu',\mathbf{k}'+\mathbf{q}} a_{\lambda',\mathbf{k}-\mathbf{q}}\rangle \\ &\quad - \langle a^\dagger_{\lambda,\mathbf{k}} a^\dagger_{\nu,\mathbf{k}'} a_{\nu',\mathbf{k}'+\mathbf{q}} a_{\lambda',\mathbf{k}-\mathbf{q}}\rangle_{\mathrm{S}}, \end{aligned} \tag{28}$$

where the factorized single-particle contributions are removed. Generally, $\Gamma_{\mathbf{k}}$ leads to the dephasing of the polarization. The corresponding phonon terms are defined by $\mathcal{D}^{\lambda,\nu}_{\mathbf{k},\mathbf{q}} \equiv \sum_{p_z} G_{p_z,\mathbf{q}}\Delta\langle\left(D_{p_z,\mathbf{q}} + D^\dagger_{p_z,\mathbf{q}}\right) a^\dagger_{\lambda,\mathbf{k}} a_{\nu,\mathbf{k}-\mathbf{q}}\rangle$. The set of equations (22–24) defines the general *semiconductor Bloch equations* (SBE).

3.1 Coherent excitons

The homogeneous solution of equation (22) without the two-particle correlations defines the eigenvalue problem

$$\tilde{\epsilon}_{\mathbf{k}}\phi^R_\lambda(\mathbf{k}) - \left(1 - f^e_{\mathbf{k}} - f^h_{\mathbf{k}}\right)\sum_{\mathbf{k}'} V_{\mathbf{k}-\mathbf{k}'}\phi^R_\lambda(\mathbf{k}') = E_\lambda\phi^R_\lambda(\mathbf{k}), \tag{29}$$

which has excitonic solutions for vanishing densities. For elevated densities, $f^e_{\mathbf{k}}$ and $f^h_{\mathbf{k}}$ are nonzero such that the problem becomes non-Hermitian. Consequently, equation (29) has both left-handed, $\phi^L_\lambda(\mathbf{k})$, and right-handed, $\phi^R_\lambda(\mathbf{k})$, solutions connected via

$$\phi^L_\lambda(\mathbf{k}) = \frac{\phi^R_\lambda(\mathbf{k})}{1 - f^e_{\mathbf{k}} - f^h_{\mathbf{k}}}, \tag{30}$$

and normalized as

$$\sum_{\mathbf{k}} \phi^L_\lambda(\mathbf{k})\phi^R_\nu(\mathbf{k}) = \delta_{\lambda,\nu}. \tag{31}$$

Expanding the polarization in the basis of these eigenfunctions, we obtain

$$P_{\mathbf{k}} = \sum_\lambda p_\lambda\phi^R_\lambda(\mathbf{k}), \qquad p_\lambda = \sum_{\mathbf{k}} \phi^L_\lambda(\mathbf{k})P_{\mathbf{k}}. \tag{32}$$

This way, equation (22) can be transformed into

$$i\hbar\frac{\partial}{\partial t}p_\lambda = E_\lambda p_\lambda - d_{vc}\phi^R_\lambda(\mathbf{r}=0)\langle E(t)\rangle - i\Gamma_\lambda, \tag{33}$$

which clearly shows that optical excitations involve only s-like states since

$$\phi^R_\lambda(\mathbf{r}=0) = \sum_{\mathbf{k}} \phi^R_\lambda(\mathbf{k}) \tag{34}$$

vanishes for states with any other symmetry. Even though equation (33) has a seemingly simple form, the consistent solution with the two-particle correlation terms Γ_λ is highly nontrivial. In practice, because of the mathematical structure of the exciton eigenfunctions, it is advantageous to numerically evaluate the full problem in the original electron-hole picture.

When the two-particle correlation terms in equations (22–24), e.g. Γ term in equation (22), can be neglected, the system is in the so-called coherent limit [1], where the excitation does not suffer from irreversible decay and we have the strict conservation law

$$\left(f_{\mathbf{k}} - \frac{1}{2}\right)^2 + |P_{\mathbf{k}}|^2 = \frac{1}{4}, \tag{35}$$

where $f_{\mathbf{k}} \equiv f^e_{\mathbf{k}} = f^h_{\mathbf{k}}$. Since the coherent limit implies that the system does not have correlations, i.e. the Hartree-Fock factorization is exact, one should be able to find the many-body wavefunction in the form of a Slater determinant. Thus, we seek for an exact wavefunction in the form of

$$|\Psi_{\mathrm{coh}}(t)\rangle = \prod_{\mathbf{k}} L^\dagger_{\mathbf{k}}(t)|\Psi_0\rangle, \tag{36}$$

where $|\Psi_0\rangle$ is the state of the unexcited semiconductor and $L^\dagger_{\mathbf{k}}$ is a fermion creation operator such that $|\Psi_{\rm coh}(t)\rangle$ is a Slater determinant. Since $|\Psi_{\rm coh}(t)\rangle$ does not lead to any correlations, the only constraint is that it should produce the correct coherent limit $f_{\mathbf{k}}$ and $P_{\mathbf{k}}$ fulfilling the condition (35). We choose the operator as

$$L^\dagger_{\mathbf{k}}(t) = e^{i\psi_{\mathbf{k}}(t)}\sin\beta_{\mathbf{k}}(t)\; a^\dagger_{c,\mathbf{k}} + \cos\beta_{\mathbf{k}}(t)\; a^\dagger_{v,\mathbf{k}}, \tag{37}$$

which has indeed fermionic character since $[L_{\mathbf{k}}, L_{\mathbf{k}'}]_+ = [L^\dagger_{\mathbf{k}}, L^\dagger_{\mathbf{k}'}]_+ = 0$ and $[L_{\mathbf{k}}, L^\dagger_{\mathbf{k}'}]_+ = \delta_{\mathbf{k},\mathbf{k}'}$. Furthermore, one directly finds that

$$f_{\mathbf{k}} = \langle a^\dagger_{c,\mathbf{k}} a_{c,\mathbf{k}}\rangle = 1 - \langle a^\dagger_{v,\mathbf{k}} a_{v,\mathbf{k}}\rangle = \sin^2\beta_{\mathbf{k}}(t), \tag{38}$$

$$P_{\mathbf{k}} = \langle a^\dagger_{v,\mathbf{k}} a_{c,\mathbf{k}}\rangle = \sin\beta_{\mathbf{k}}(t)\,\cos\beta_{\mathbf{k}}(t)\; e^{i\psi_{\mathbf{k}}(t)}. \tag{39}$$

By using the basic properties of the trigonometric functions, it is easy to see that equations (38) and (39) fulfill the coherent-limit condition (35). The explicit values of $\beta_{\mathbf{k}}(t)$ and $\psi_{\mathbf{k}}(t)$ are fixed by the inverse of equations (38) and (39), i.e.,

$$\beta_{\mathbf{k}}(t) = \arcsin\sqrt{f_{\mathbf{k}}}, \tag{40}$$

$$e^{i\psi_{\mathbf{k}}(t)} = \frac{P_{\mathbf{k}}}{|P_{\mathbf{k}}|}. \tag{41}$$

Since the coherent limit can also be presented in the exciton basis, i.e. equation (32), it is worthwhile to study how excitonic features enter the exact wavefunction equation (36). For this purpose, it is convenient to introduce an exciton operator

$$X_{\lambda,\mathbf{q}} \equiv \sum_{\mathbf{k}} \phi^R_\lambda(\mathbf{k}) a^\dagger_{v,\mathbf{k}-\mathbf{q}_h} a_{c,\mathbf{k}+\mathbf{q}_e}, \tag{42}$$

containing the center-of-mass momentum and $\mathbf{q}_{e(h)} = (m_{e(h)}/(m_e+m_h))\mathbf{q}$ [18]. Its inverse transformation back to the electron-hole picture follows from

$$a^\dagger_{v,\mathbf{k}-\mathbf{q}_h} a_{c,\mathbf{k}+\mathbf{q}_e} = \sum_\lambda \phi^L_\lambda(\mathbf{k}) X_{\lambda,\mathbf{q}}, \tag{43}$$

where we used the completeness relation, $\sum_\lambda \phi^L_\lambda(\mathbf{k})\phi^R_\lambda(\mathbf{k}) = \delta_{\mathbf{k},\mathbf{k}'}$. Next, we introduce the operator

$$S = \sum_\lambda \left[c^\star_\lambda X_{\lambda,0} - c_\lambda X^\dagger_{\lambda,0}\right]. \tag{44}$$

This operator has the interesting property that

$$\begin{aligned} e^S a^\dagger_{v,\mathbf{k}} e^{-S} &= a^\dagger_{v,\mathbf{k}} + \left[S, a^\dagger_{v,\mathbf{k}}\right]_- + \frac{1}{2!}\left[S, \left[S, a^\dagger_{v,\mathbf{k}}\right]_-\right]_- + \ldots \\ &= e^{i\psi_{\mathbf{k}}(t)}\sin\beta_{\mathbf{k}}(t) a^\dagger_{c,\mathbf{k}} + \cos\beta_{\mathbf{k}}(t)\; a^\dagger_{v,\mathbf{k}} \\ &= L^\dagger_{\mathbf{k}}(t), \end{aligned} \tag{45}$$

produces the fermionic $L^\dagger_{\mathbf{k}}(t)$ operator when we make the identification

$$e^{i\psi_{\mathbf{k}}(t)}\beta_{\mathbf{k}}(t) \equiv \sum_\lambda c_\lambda(t)\phi^R_\lambda(\mathbf{k}). \tag{46}$$

Consequently, we can write $L^\dagger_{\mathbf{k}}(t) = e^S a^\dagger_{v,\mathbf{k}} e^{-S}$. Using this general connection, the coherent-limit wavefunction can then be expressed as

$$\begin{aligned} |\Psi_{\rm coh}(t)\rangle &= \prod_{\mathbf{k}} \left(e^S a^\dagger_{v,\mathbf{k}} e^{-S}\right)|\Psi_0\rangle = e^S\left(\prod_{\mathbf{k}} a^\dagger_{v,\mathbf{k}}\right) e^{-S}|\Psi_0\rangle \\ &= e^S \prod_{\mathbf{k}} a^\dagger_{v,\mathbf{k}}|\Psi_0\rangle, \end{aligned} \tag{47}$$

since $e^S e^{-S} = 1$ and $e^{-S}|\Psi_0\rangle = |\Psi_0\rangle$. Form this form, we also observe that $\prod_{\mathbf{k}} a^\dagger_{v,\mathbf{k}}|\Psi_0\rangle \equiv |\Psi_G\rangle$ is the ground state of a semiconductor where the valence band is completely filled. Thus, the coherent state can equivalently be presented by

$$|\Psi_{\rm coh}(t)\rangle = e^S|\Psi_G\rangle, \tag{48}$$

which indicates that the operator e^S generates the coherent limit.

To study the coherent limit in more detail, we determine a functional

$$D[c] \equiv e^{S[c]} = e^{\sum_\lambda\left(c^\star_\lambda X_{\lambda,0} - c_\lambda X^\dagger_{\lambda,0}\right)}, \tag{49}$$

which generates the coherent-limit wavefunction, $|\Psi_{\rm coh}(t)\rangle = D[c]|\Psi_G\rangle$, according to equation (48). The functional form of D resembles the displacement operator [19] generating coherent states for fully bosonic fields. Due to this formal analogy, one can define that $|\Psi_{\rm coh}(t)\rangle$ defines *coherent excitons*. However, one should note that the operator $X_{\lambda,0}$ is fundamentally non-bosonic [20] such that $|\Psi_{\rm coh}(t)\rangle$ cannot be interpreted as a bosonic exciton. Moreover, $|\Psi_{\rm coh}(t)\rangle$ is still a Slater determinant of single-electron functions in a conduction-valence-band superposition state. Hence, a *coherent exciton is not a truly bound electron-hole pair* which must be — by definition — a correlated two-particle electron-hole-pair object.

A proper interpretation of coherent excitons is obtained via equations (36) and (37) showing the full fermionic substructure. One sees that a coherent exciton is nothing but a state where any single carrier with momentum $\mathbf{k}$ is in a superposition state between the conduction and valence band. At the same time, the different carriers are completely uncorrelated; only the conduction-valence band mixture of each carrier is given by a collective phase and amplitude determined by β and ψ.

3.2 Elliot formula

Before we discuss the microscopic correlation contributions to the SBE, we first summarize the analytic solution of the linear problem using a phenomenological expression for Γ [1]. This allows us to identify the principal effects beyond the coherent limit. To simplify the analysis, we start from an incoherent semiconductor system, i.e., all polarizations vanish before the system is excited, and study the linear response by linearizing the SBE. In this linear limit, $f^e_{\mathbf{k}}$ and $f^h_{\mathbf{k}}$ remain zero while only a small — linear —

polarization $P_{\mathbf{k}}$ is generated. When the microscopic Γ is replaced by a phenomenological value γp_λ, equation (33) reduces to

$$\hbar\omega p_\lambda(\omega) = (E_\lambda - i\gamma)\, p_\lambda(\omega) - d_{vc}\phi^R_\lambda(r=0)\langle E(\omega)\rangle, \quad (50)$$

where we Fourier-transformed to the frequency space. The solution of this equations yields the Elliot formula [21] for the linear semiconductor susceptibility

$$\chi(\omega) = \frac{\sum_\lambda d_{cv}\phi^R_\lambda(r=0)p_\lambda(\omega)}{\langle E(\omega)\rangle} = |d_{cv}|^2 \sum_\lambda \frac{|\phi^R_\lambda(r=0)|^2}{E_\lambda - \hbar\omega - i\gamma}, \quad (51)$$

which shows that absorption resonances occur at the frequencies $\omega = E_\lambda/\hbar$.

3.3 Excitation-induced dephasing

The analysis shows that the Elliot formula remains structurally unchanged when the microscopic correlation contributions Γ in equation (33) are microscopically evaluated. However, in this case (i) γ becomes dependent on both ω and exciton state λ; (ii) higher energy exciton states experience a larger γ; (iii) γ increases for elevated carrier densities, which leads to the so-called excitation-induced dephasing, and (iv) one finds density-, exciton-index, and frequency-dependent renormalizations of both E_λ and $\phi_\lambda(r=0)$ [22,23].

To illustrate theses effects, we evaluate $\chi(\omega)$ numerically including the fully microscopic Coulomb scattering while a bath approximation [15] is applied for phonons. We use two geometrically different GaAs-type semiconductor systems: (i) a 8 nm quantum well; and (ii) a planar arrangement of identical quantum wires. The quantum wires are placed such that they are much closer than the relevant optical wave length but, at the same time, they are so far apart that the different wires are not electronically coupled. In this situation, each quantum wire is electronically independent and optical effects do not lead to a diffraction pattern. Consequently, the quantum-wire arrangement is as close as possible to the quantum well. As a major computational advantage, the quantum-wire arrangement leads to a significantly reduced numerical effort since it has much smaller dimensional correlations and integrals compared to the quantum-well systems. We choose the standard GaAs-type parameters for the quantum well and wire [18] such that the three-dimensional Bohr radius is $a_0 = 12.5$ nm and the corresponding binding energy is $E_B = 4.2$ meV. The sizes of the wire and well are taken such that they produce the same energy separation between the two lowest exciton states. The lattice temperature is assumed to be low such that it is sufficient to include only acoustic phonons [15].

Figure 1 shows the computed absorption spectra for a quantum well (upper frame) and quantum wire (lower frame) for four representative carrier densities. The carriers are assumed to be in 40 K Fermi-Dirac distributions;

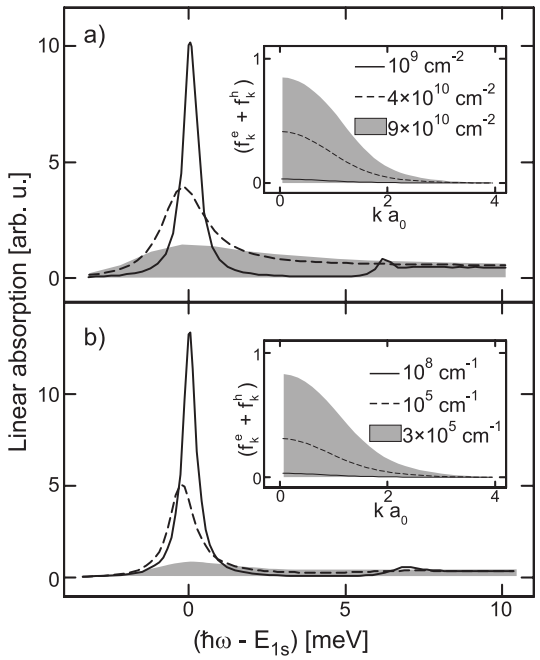

Fig. 1. Linear absorption spectra for (a) a quantum-well and (b) a quantum-wire system at different carrier densities following 40 K Fermi-Dirac distributions. The insets show the corresponding $(f^e + f^h)$.

$(f^e_{\mathbf{k}} + f^h_{\mathbf{k}})$ is shown as an inset. In both cases, the lowest density (10^9 cm^{-2} for the well and 10^4 cm^{-1} for the wire) show a rather similar $(f^e_{\mathbf{k}} + f^h_{\mathbf{k}})$ which is always much below unity. Consequently, both cases have clear absorption resonances at the $1s$- and at the $2s$-energy. At the same time, we notice that the $2s$ resonance is broader already at these moderate densities, which verifies that the excitation-induced dephasing rapidly becomes stronger for higher lying excitons states. For elevated densities, also the $1s$ resonance is broadened. Even though the corresponding $(f^e_{\mathbf{k}} + f^h_{\mathbf{k}})$ is still relatively low, the $2s$ and higher excitons are bleached. As a general feature for both well and wire, we see that the spectral $1s$ position remains almost unchanged indicating that the microscopic scattering leads to energy renormalizations which compensate the Hartree-Fock shifts. As the density is increased to 9×10^{10} cm^{-2} for the well and 3×10^5 cm^{-1} for the wire, we see that the $1s$ resonance is nearly completely bleached. In both cases, the corresponding $(f^e_{\mathbf{k}} + f^h_{\mathbf{k}})$ is close to unity, indicating strong phase-space filling effects which eventually prevent the possibility to have bound exciton states. Only ionized exciton states are allowed beyond this Mott transition [24].

4 Conversion of polarization into excitons

When the correlation terms become important, the coherent polarization can decay into incoherent correlations which may contain true excitons. The exciton correlation

is determined by $c_{\rm X}^{\mathbf{q},\mathbf{k}',\mathbf{k}} \equiv c_{c,v,c,v}^{\mathbf{q},\mathbf{k}',\mathbf{k}}$ and its singlet-doublet dynamics is determined from [5,18,25]

$$\begin{aligned} i\hbar\frac{\partial}{\partial t}c_{\rm X}^{\mathbf{q},\mathbf{k}',\mathbf{k}} = {} & \epsilon^{\mathbf{q},\mathbf{k}',\mathbf{k}}c_{\rm X}^{\mathbf{q},\mathbf{k}',\mathbf{k}} + S^{\mathbf{q},\mathbf{k}',\mathbf{k}} \\ & + \left(1-f_{\mathbf{k}}^{e}-f_{\mathbf{k}-\mathbf{q}}^{h}\right)\sum_{\mathbf{l}}V_{\mathbf{l}-\mathbf{k}}c_{\rm X}^{\mathbf{q},\mathbf{k}',\mathbf{l}} \\ & - \left(1-f_{\mathbf{k}'+\mathbf{q}}^{e}-f_{\mathbf{k}'}^{h}\right)\sum_{\mathbf{l}}V_{\mathbf{l}-\mathbf{k}'}c_{\rm X}^{\mathbf{q},\mathbf{l},\mathbf{k}} \\ & + iG^{\mathbf{q},\mathbf{k}',\mathbf{k}} + D_{\rm rest}^{\mathbf{q},\mathbf{k}',\mathbf{k}} + T^{\mathbf{q},\mathbf{k}',\mathbf{k}}, \end{aligned} \tag{52}$$

with

$$\begin{aligned} iG^{\mathbf{q},\mathbf{k}',\mathbf{k}} = {} & \left(P_{\mathbf{k}}^{\star}-P_{\mathbf{k}-\mathbf{q}}^{\star}\right)\left[V_{\mathbf{q}}\sum_{\mathbf{n},\lambda}c_{v,\lambda,\lambda,c}^{-\mathbf{q},\mathbf{n},\mathbf{k}'}-\mathcal{D}_{\mathbf{k}',-\mathbf{q}}^{v,c}\right] \\ & + \left(P_{\mathbf{k}'}-P_{\mathbf{k}'+\mathbf{q}}\right)\left[V_{\mathbf{q}}\sum_{\mathbf{n},\lambda}c_{c,\lambda,\lambda,v}^{\mathbf{q},\mathbf{n},\mathbf{k}}-\mathcal{D}_{\mathbf{k},\mathbf{q}}^{c,v}\right]. \end{aligned} \tag{53}$$

The different contributions describe the renormalized kinetic energy $\epsilon^{\mathbf{q},\mathbf{k}',\mathbf{k}}$ and single-particle source S which has the typical Coulomb scattering form $V\left[f_1f_2\left(1-f_3\right)\left(1-f_4\right)-\left(1-f_1\right)\left(1-f_2\right)f_3f_4\right]$. The Coulomb sums with the phase-space filling factor $(1-f^e-f^h)$ describe the attractive interaction between electrons and holes, allowing them to become truly bound electron-hole pairs, i.e. *incoherent excitons*. The G term contains the same $c_{v,\lambda,\lambda,c}$ and $\mathcal{D}^{v,c}$ correlations as Γ in equation (27), showing how coherent excitons are converted into $c_{\rm X}^{\mathbf{q},\mathbf{k}',\mathbf{k}}$ correlations which can include true incoherent excitons. The remaining two-particle contributions are denoted as $D_{\rm rest}$ while T symbolizes the three-particle Coulomb and phonon terms treated here at the scattering level. Also the other correlations, $c_{\lambda,\nu,\nu',\lambda'}^{\mathbf{q},\mathbf{k}',\mathbf{k}}$ have a structurally similar dynamics as equation (53). In the numerical solutions, we treat all of them together with the corresponding equations for the singlets. This way, we fully include one- and two-particle correlations and obtain a closed set of equations providing a consistent description of optical excitations in semiconductors. Once again, the phonons are treated as a bath set to the lattice temperature, the corresponding scattering terms are given in references [15,18].

4.1 Incoherent excitons

Like the polarization, also the correlation $c_{\rm X}^{\mathbf{q},\mathbf{k}',\mathbf{k}}$ can be expressed in the exciton basis using

$$\Delta\langle X_{\lambda,\mathbf{q}}^{\dagger}X_{\nu,\mathbf{q}}\rangle = \sum_{\mathbf{k},\mathbf{k}'}\phi_{\lambda}^{L}(\mathbf{k})\phi_{\nu}^{L}(\mathbf{k}')c_{\rm X}^{\mathbf{q},\mathbf{k}'-\mathbf{q}_h,\mathbf{k}+\mathbf{q}_e} \tag{54}$$

$$c_{\rm X}^{\mathbf{q},\mathbf{k}'-\mathbf{q}_h,\mathbf{k}+\mathbf{q}_e} = \sum_{\lambda,\nu}\phi_{\lambda}^{R}(\mathbf{k})\phi_{\nu}^{R}(\mathbf{k}')\Delta\langle X_{\lambda,\mathbf{q}}^{\dagger}X_{\nu,\mathbf{q}}\rangle. \tag{55}$$

By applying equation (55) in equation (52), we obtain

$$\begin{aligned} i\hbar\frac{\partial}{\partial t}\Delta\langle X_{\lambda,\mathbf{q}}^{\dagger}X_{\nu,\mathbf{q}}\rangle = {} & \left(E_{\nu}-E_{\lambda}\right)\Delta\langle X_{\lambda,\mathbf{q}}^{\dagger}X_{\nu,\mathbf{q}}\rangle \\ & + \left(E_{\nu}-E_{\lambda}\right)\langle X_{\lambda,\mathbf{q}}^{\dagger}X_{\nu,\mathbf{q}}\rangle_{\rm S} \\ & + iG^{\lambda,\nu}(\mathbf{q}) + D_{\rm rest}^{\lambda,\nu}(\mathbf{q}) + T^{\lambda,\nu}(\mathbf{q}), \end{aligned} \tag{56}$$

where the singlet scattering, $S^{\mathbf{q},\mathbf{k}',\mathbf{k}}$, in equation (52) leads to a source

$$\langle X_{\lambda,\mathbf{q}}^{\dagger}X_{\nu,\mathbf{q}}\rangle_{\rm S} = \sum_{\mathbf{k}}\phi_{\lambda}^{L}(\mathbf{k})f_{\mathbf{k}+\mathbf{q}_e}^{e}f_{\mathbf{k}-\mathbf{q}_h}^{h}\phi_{\nu}^{L}(\mathbf{k}). \tag{57}$$

The other sources are expressed symbolically as $G^{\lambda,\nu}(\mathbf{q})$, $D_{\rm rest}^{\lambda,\nu}(\mathbf{q})$, and $T^{\lambda,\nu}(\mathbf{q})$.

If we assume completely incoherent conditions, $G^{\lambda,\nu}(\mathbf{q})$ vanishes. In addition, if we introduce an approximation where $D_{\rm rest}^{\lambda,\nu}(\mathbf{q})$ is neglected while the triple scattering is described phenomenologically via $T^{\lambda,\nu}(\mathbf{q}) = -i\gamma\Delta\langle X_{\lambda,\mathbf{q}}^{\dagger}X_{\nu,\mathbf{q}}\rangle$, we find a simple steady-state solution

$$\Delta\langle X_{\lambda,\mathbf{q}}^{\dagger}X_{\nu,\mathbf{q}}\rangle = -\frac{E_{\nu}-E_{\lambda}}{E_{\nu}-E_{\lambda}-i\gamma}\langle X_{\lambda,\mathbf{q}}^{\dagger}X_{\nu,\mathbf{q}}\rangle_{\rm S}, \tag{58}$$

provided that the carrier densities remain constant. We notice that we have no true exciton populations, i.e. the diagonal contributions $\Delta\langle X_{\lambda,\mathbf{q}}^{\dagger}X_{\lambda,\mathbf{q}}\rangle$ vanish. Consequently, true exciton populations can be generated only if (i) triplet scattering is described microscopically [18] or (ii) a coherent polarization is converted into populations via the $G^{\lambda,\nu}(\mathbf{q})$ term [25].

Next, we investigate the polarization-to-population conversion via the full numerical solutions of the singlet-doublet equations. Since, $G^{\lambda,\nu}(\mathbf{q})$, $D_{\rm rest}^{\lambda,\nu}(\mathbf{q})$, and $T^{\lambda,\nu}(\mathbf{q})$ contain genuine fermion correlations, like density-polarization and density-density correlations, the consistent analysis must be performed in the original electron-hole picture. However, from the results of these computations, we can directly construct true exciton properties via the transformation (55). Especially, we can determine the momentum distribution and density [5,18] of a specific ν exciton by using

$$\Delta N_{\nu}(\mathbf{q}) \equiv \Delta\langle X_{\nu,\mathbf{q}}^{\dagger}X_{\nu,\mathbf{q}}\rangle \tag{59}$$

$$\Delta n_{\nu} = \frac{1}{\mathcal{L}^{d}}\sum_{\mathbf{q}}\Delta N_{\nu}(\mathbf{q}), \tag{60}$$

respectively.

Due to the numerical complexity of the coupled equations, we perform the full computation only for the quantum-wire system. To study the generation of incoherent excitons in their different quantum states, we assume pulsed optical excitation resonant with either the $1s$- or $2s$-resonance; the lattice temperature is 4 K. We repeat the computations for two different pump intensities and evaluate the evolution of the exciton density Δn_{ν} relative to the generated carrier density $n = (1/\mathcal{L}^{d})\sum_{k} f_{\mathbf{k}}^{e(h)}$.

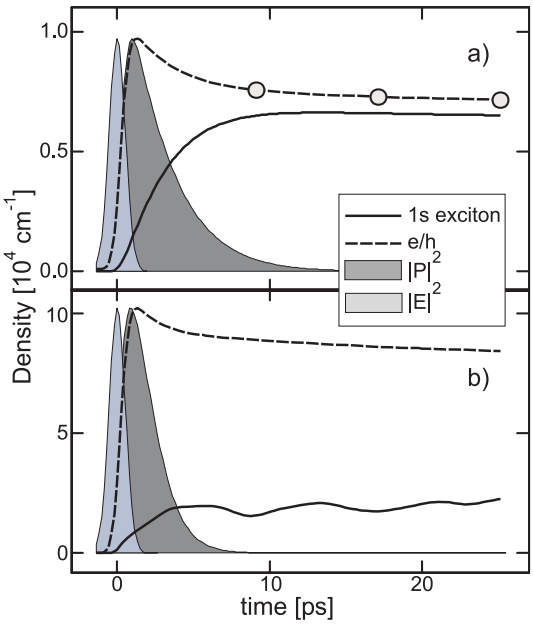

Fig. 2. System dynamics after excitation at the 1s-exciton resonance for (a) a low and (b) an intermediate pump intensity. Plotted are the excitation pulse (light shaded area), the generated $|P|^2$ (dark shaded line), the carrier density (dashed line), and the 1s-exciton density (solid line). The circles denote the time moments for which further results are shown in Figures 6, 7, and 9.

4.2 Resonant 1s excitation

When the semiconductor is excited resonantly, one first obtains coherent excitons, i.e. polarization which then may be converted into true excitons. In order to determine the corresponding dynamics, we investigate resonant 1s excitation assuming two different intensities for the pulsed optical excitation. In Figure 2, we show the excitation pulse (bright shaded area), the computed polarization (dark shaded area), the carrier density (dashed line), and the 1s-exciton density (solid line). We compare the results for a low excitation intensity (Fig. 2a) and an intermediate intensity (Fig. 2b). For the low excitation, the polarization decays on a 2.8 ps scale and we reach a carrier density of 10^4 cm^{-1}, whereas for the intermediate density we find a more rapid decay time of 1.9 ps and a density approaching 10^5 cm^{-1}. The decay times are in good agreement with the corresponding line width of the linear absorption of Figure 1. Thus, we conclude that the higher excitation decays faster due to the elevated excitation-induced dephasing. As the polarization decays, it clearly becomes converted into true 1s-exciton populations. For the lower excitation, the conversion efficiency is above 90%. This large conversion fraction is expected since coherent and incoherent 1s-excitons have an excellent energetic match. However, the elevated intensity excitation produces only around 25% conversion event though the excitation is still relatively weak. As the excitation is increased further, the conversion drops to zero thanks to the fermionic substructure of the excitons [24,25].

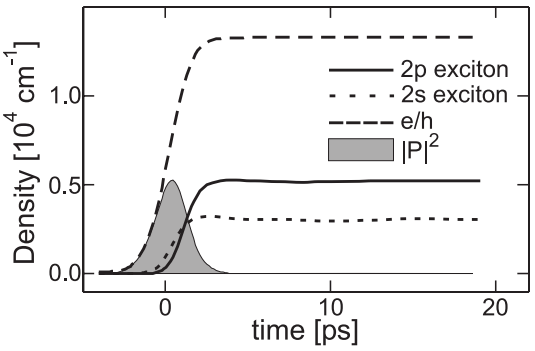

Fig. 3. System dynamics following an excitation at the 2s-exciton resonance. Plotted are $|P|^2$ (shaded area), the carrier density (dashed line), the 2s-exciton density (dotted line), and the 2p-exciton density (solid line).

4.3 Resonant 2s excitation

The results of calculations done for excitation at the 2s-exciton resonance are presented in Figure 3. Here, we have used a 2 ps long excitation pulse the computed polarization (shaded area) practically follows its temporal evolution; also the corresponding carrier density (dashed line) as well as the exciton densities n_{2s} (dotted line) and n_{2p} (solid line) are shown. In the one-dimensional quantum wire, 2p-exciton corresponds to the lowest exciton with an odd symmetry $\phi_{2p}(-k) = -\phi_{2p}(k)$; it is practically degenerate with the symmetric 2s-exciton in analog to the two-dimensional system. Figure 3 shows that the generated polarization decays rather fast on a sub 1 ps scale even though the carrier density is below $10^4\,\mathrm{cm}^{-1}$. This is again a consequence of the fact that the excitation-induced dephasing is much stronger for the 2s than for the 1s resonance as discussed in Section 3.3. As the polarization decays, *the 2s-polarization is converted into a mix of 2s and 2p populations*, which is not unexpected from the point of view of the conservation of energy. However, the significant generation of p-type excitons might be unexpected at first sight since it involves a symmetry change of the optically generated s-type polarization.

In the case of 2s pumping, the polarization-to-population conversion is dominantly mediated via the Coulomb scattering [25]. In order to understand how the Coulomb interaction induces symmetry changes in the polarization conversion, we now investigate the scattering (Γ) and the conversion (G) mechanisms which stem from the same fermionic correlation $c_{v,\lambda,\lambda,c} = \Delta\langle a_v^\dagger a_\lambda^\dagger a_\lambda a_c\rangle$ between polarization and fermionic density. Consequently, the specific form of the polarization decay fully determines the corresponding conversion in excitonic population.

As a first test, we make the simplest possible phenomenological approximation

$$\left[V_{\mathbf{q}} \sum_{\mathbf{n},\lambda} c^{\mathbf{q},\mathbf{n},\mathbf{k}}_{v,\lambda,\lambda,c}\right]_{\text{app.}} = i\frac{\gamma}{2} P_{\mathbf{k}} \delta_{\mathbf{q},0}. \qquad (61)$$

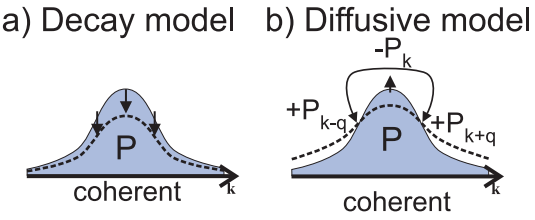

Fig. 4. Schematic presentation of two polarization-to-population conversion schemes: (a) via the dephasing model described by equations (62) and (63) and (b) via the diffusive model described by equations (67) and (68).

By inserting this into equations (27) and (53), we find a decay model

$$i\Gamma_{\mathbf{k}}^{\mathrm{app}} = \sum_{\mathbf{q}} \left[V_{\mathbf{q}} \sum_{\mathbf{n},\lambda} c_{v,\lambda,\lambda,c}^{\mathbf{q},\mathbf{n},\mathbf{k}} \right]_{\mathrm{app}} - [c \leftrightarrow v]^{\star} = i\gamma P_{\mathbf{k}}, \quad (62)$$

$$iG_{\mathrm{app.}}^{\mathbf{q},\mathbf{k}',\mathbf{k}} = 2iP_{\mathbf{k}}^{\star}\Gamma P_{\mathbf{k}'}\,\delta_{\mathbf{q},0}. \quad (63)$$

These approximations conserve the property that $[P_{\mathbf{k}}^{\star}P_{\mathbf{k}'} + \sum_{\mathbf{q}} c_X^{\mathbf{q},\mathbf{k}',\mathbf{k}}]$ is a constant of motion with respect to the scattering such that polarization-to-population conversion is properly described. However, this model only allows for conversion of s-type polarization to s-like exciton populations, in contrast to our microscopic results. The corresponding polarization-to-population conversion is schematically illustrated in Figure 4a.

For a better approximation, we look at the process of excitation-induced dephasing [14]. We notice that Coulomb induced dephasing is actually a diffusive redistribution of the microscopic polarizations since it satisfies strict conservation laws

$$\sum_{\mathbf{k}} \Gamma_{\mathbf{k}} = 0 \quad (64)$$

$$\sum_{\mathbf{k},\mathbf{k}',\mathbf{q}} G^{\mathbf{q},\mathbf{k}',\mathbf{k}} = 0. \quad (65)$$

Clearly, our first approximation violates these conditions. In order to analyze the consequences of these fundamental restrictions, we use a somewhat reduced model which still has the same structural form as the second-Born solution of $c_{v,\lambda,\lambda,c}$ [14]. We approximate

$$\left[V_{\mathbf{q}} \sum_{\mathbf{n},\lambda} c_{v,\lambda,\lambda,c}^{\mathbf{q},\mathbf{n},\mathbf{k}} \right]_{\mathrm{red.}} = iU_{\mathbf{q}}(P_{\mathbf{k}} - P_{\mathbf{k}-\mathbf{q}})/2, \quad (66)$$

where $U_{\mathbf{q}}$ is chosen to be a real-valued, nonlinear functional of f and P. By inserting this into equations (27) and (53), we find a diffusive model

$$\begin{aligned} i\Gamma_{\mathbf{k}}^{\mathrm{red}} &= \sum_{\mathbf{q}} \left[V_{\mathbf{q}} \sum_{\mathbf{n},\lambda} c_{v,\lambda,\lambda,c}^{\mathbf{q},\mathbf{n},\mathbf{k}} \right]_{\mathrm{red}} - [c \leftrightarrow v]^{\star} \\ &= i \sum_{\mathbf{q}} U_{\mathbf{q}}(P_{\mathbf{k}-\mathbf{q}} - P_{\mathbf{q}}), \end{aligned} \quad (67)$$

$$\begin{aligned} iG_{\mathrm{red}}^{\mathbf{q},\mathbf{k}',\mathbf{k}} &= (P_{\mathbf{k}}^{\star} - P_{\mathbf{k}-\mathbf{q}}^{\star}) \left[V_{\mathbf{q}} \sum_{\mathbf{n},\lambda} c_{v,\lambda,\lambda,c}^{-\mathbf{q},\mathbf{n},\mathbf{k}'} \right]_{\mathrm{red.}} \\ &\quad - (P_{\mathbf{k}'+\mathbf{q}} - P_{\mathbf{k}'}) \left[V_{\mathbf{q}} \sum_{\mathbf{n},\lambda} c_{v,\lambda,\lambda,c}^{\mathbf{q},\mathbf{n},\mathbf{k}} \right]_{\mathrm{red.}}^{\star} \\ &= i(P_{\mathbf{k}}^{\star} - P_{\mathbf{k}-\mathbf{q}}^{\star}) U_{\mathbf{q}} (P_{\mathbf{k}'+\mathbf{q}} - P_{\mathbf{k}'}), \end{aligned} \quad (68)$$

which both obey the conservation laws (64–65). The corresponding polarization-to-population conversion is schematically illustrated in Figure 4b. We observe that $\Gamma_{\mathbf{k}}^{\mathrm{red}}$ removes polarization from the state $P_{\mathbf{k}}$ and redistributes it to $P_{\mathbf{k}-\mathbf{q}}$. A slightly more complicated redistribution is observed for populations.

Due to the relatively simple form of G_{red}, we may now express it in the exciton basis. Especially, the the conversion rate to the exciton state ν becomes

$$\begin{aligned} G_{\mathrm{red}}^{\nu,\nu}(\mathbf{q}) &= \sum_{\mathbf{k},\mathbf{k}'} \phi_{\nu}^{L}(\mathbf{k}) \phi_{\nu}^{L}(\mathbf{k}') G_{\mathrm{red}}^{\mathbf{q},\mathbf{k}'-\mathbf{q}_h,\mathbf{k}+\mathbf{q}_e} \\ &= |M_{\nu}(\mathbf{q})|^2 f_{\mathbf{q}}, \end{aligned} \quad (69)$$

$$M_{\nu}(\mathbf{q}) \equiv \sum_{\mathbf{k}} \phi_{\nu}^{L}(\mathbf{k}) \left[P_{\mathbf{k}+\mathbf{q}_e} - P_{\mathbf{k}-\mathbf{q}_h} \right], \quad (70)$$

indicating that Coulomb scattering leads to the generation of excitons with finite momenta, but no population in the $\mathbf{q} = 0$ state is produced. For low to moderate $2s$ excitation, we may use the approximation $P_{\mathbf{k}} \propto \phi_{2s}^{R}(\mathbf{k})$. With the help of the symmetries $\phi_{2s}^{R}(-\mathbf{k}) = \phi_{2s}^{R}(\mathbf{k})$ and $\phi_{2p}^{R}(-\mathbf{k}) = -\phi_{2p}^{R}(\mathbf{k})$, we find that $2s$- and $2p$-generation rates follow from

$$M_{2s}(\mathbf{q}) \propto \sum_{\mathbf{k}} \phi_{2p}^{L}(\mathbf{k}) \left[\phi_{2s}^{R}(\mathbf{k}+\mathbf{q}_e) - \phi_{2s}^{R}(\mathbf{k}+\mathbf{q}_h) \right], \quad (71)$$

$$M_{2p}(\mathbf{q}) \propto \sum_{\mathbf{k}} \phi_{2p}^{L}(\mathbf{k}) \left[\phi_{2s}^{R}(\mathbf{k}+\mathbf{q}_e) + \phi_{2s}^{R}(\mathbf{k}+\mathbf{q}_h) \right]. \quad (72)$$

which both vanish for $\mathbf{q} = 0$ but become clearly nonzero for $\mathbf{q} \neq 0$.

For $2s$ pumping, the energy conservation aspects of $U_{\mathbf{q}}$ are practically the same for $2s$ and $2p$ since these states are nearly degenerate. As a result, the overlap of the wavefunctions with shifted arguments in $M_{\nu}(\mathbf{q})$ determines the conversion rate such that $|M_{\nu}(\mathbf{q})|^2$ can be used to estimate the ratio of generated $2s$ and $2p$ populations. The $\mathbf{q}$ dependency of $|M_{2s}(\mathbf{q})|^2$ (dashed line) and $|M_{2p}(\mathbf{q})|^2$ (solid line) are shown in Figures 5a and 5b for the quantum well (wire) by using the low-density exciton wavefunction. The computed $2p$ distribution is shown in Figure 5c for the wire after the polarization-to-population

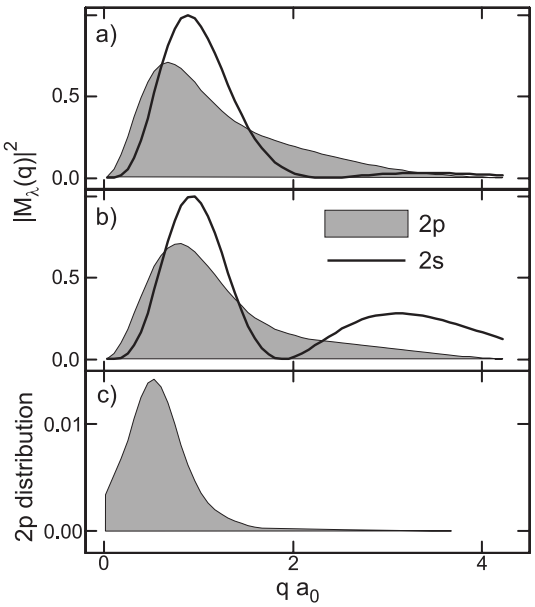

Fig. 5. Analytically computed $|M_{2s}(\mathbf{q})|^2$ (solid line) and $|M_{2p}(\mathbf{q})|^2$ (shaded area) for (a) a quantum well and (b) a quantum wire. (c) The numerically computed $2p$ distribution at the final time moment of Figure 3.

conversion is complete. We observe that the approximative analysis produces qualitatively similar distribution as the full computation. In addition, the quantum-well and wire estimates are very close to each other. If we assume that the $\mathbf{q}$ dependence of $U_\mathbf{q}$ can be ignored, $\sum_\mathbf{q} |M_{2s}(\mathbf{q})|^2$ and $\sum_\mathbf{q} |M_{2p}(\mathbf{q})|^2$ describes the relative conversion into $2s$ and $2p$-excitons, respectively. The approximative description of conversion produces a ratio of 1.36 of $2s$ over $2p$ population for the quantum wire, which is close to the numerical result in Figure 3a. Repeating the same calculations for the quantum well, we get a ratio 0.99 showing that the generation of p-like states is strong and qualitatively similar for quantum wells and wires.

Since the Coulomb interaction conserves the angular momentum, one may ask how this conservation law is fulfilled when a $2s$ polarization is converted into $2p$-excitons. This problem is easily answered by noting that we have a many-body system where only the total angular momentum is conserved. As a simplified example, we can consider a many-body state consisting of two perfect $2p$-excitons. Thus, one exciton may be in a quantum state $|\phi_{n,m}\rangle$ with the usual quantum numbers $n = 1$, $m = \pm 1$ for $2p$-excitons. Using the Clebsch-Gordan coefficients for a two-dimensional system, we may construct a two-exciton state with total ($J = 0$, $J_z = 0$)

$$|\Psi_{0,0}\rangle = \frac{1}{\sqrt{2}}[|\phi_{1,m=+1}\rangle_1 |\phi_{1,m=-1}\rangle_2 + |\phi_{1,m=-1}\rangle_1 |\phi_{1,m=+1}\rangle_2], \quad (73)$$

showing that the many-body system can generate individual p-excitons even though the total angular momentum remains in an s-like state.

5 Semiconductor luminescence equations

The optically generated semiconductor excitation can recombine spontaneously due to the vacuum-field fluctuations of the light field. To fully describe this aspect, we have to quantize the light field. For this purpose, we apply the cluster-expansion and investigate the semiconductor luminescence. The incoherent light emission follows from the photon-number type doublets $\Delta\langle B^\dagger B\rangle$. For the planar structures studied here, we separate q_z and the in-plane momentum $\mathbf{q}$ and find

$$i\hbar\frac{\partial}{\partial t}\Delta\langle B^\dagger_{q_z,\mathbf{q}} B_{q'_z,\mathbf{q}}\rangle = \hbar(\omega_{q'} - \omega_q)\,\Delta\langle B^\dagger_{q_z,\mathbf{q}} B_{q'_z,\mathbf{q}}\rangle + i\sum_\mathbf{k}[\mathcal{F}_q \Delta\langle B_{q'_z,\mathbf{q}} a^\dagger_{c,\mathbf{k}} a_{v,\mathbf{k}-\mathbf{q}}\rangle + \mathcal{F}^\star_{q'}\Delta\langle B^\dagger_{q_z,\mathbf{q}} a^\dagger_{v,\mathbf{k}-\mathbf{q}} a_{c,\mathbf{k}}\rangle]. \quad (74)$$

This equation shows that $\Delta\langle B^\dagger B\rangle$ is coupled to an amplitude $\Delta\langle B^\dagger a^\dagger_v a_c\rangle$ which describes correlations in a process where an electron is lowered from the conduction to the valence band under simultaneous emission of a photon. The corresponding correlation dynamics follows from

$$i\hbar\frac{\partial}{\partial t}\Delta\langle B^\dagger_{q_z,\mathbf{q}} a^\dagger_{v,\mathbf{k}-\mathbf{q}} a_{c,\mathbf{k}}\rangle = (\tilde\epsilon_\mathbf{k}(\mathbf{q}) - \hbar\omega_q)\Delta\langle B^\dagger_{q_z,\mathbf{q}} a^\dagger_{v,\mathbf{k}-\mathbf{q}} a_{c,\mathbf{k}}\rangle - \left[1 - f^e_\mathbf{k} - f^h_{\mathbf{k}-\mathbf{q}}\right]\Omega_{\rm ST}(\mathbf{k}; q_z, \mathbf{q}) + i\mathcal{F}_{q_z,\mathbf{q}}\left[f^e_\mathbf{k} f^h_{\mathbf{k}-\mathbf{q}} + \sum_\mathbf{l}\Delta\langle a^\dagger_{c,\mathbf{l}+\mathbf{q}} a^\dagger_{v,\mathbf{k}-\mathbf{q}} a_{c,\mathbf{k}} a_{v,\mathbf{l}}\rangle\right] + D^{coh}_{\mathbf{k},\mathbf{q}} + T_{\mathbf{k},\mathbf{q}} \quad (75)$$

where we have defined the renormalized kinetic energy

$$\tilde\epsilon_\mathbf{k}(\mathbf{q}) \equiv \tilde\epsilon^e_\mathbf{k} + \tilde\epsilon^h_{\mathbf{k}-\mathbf{q}} - \sum_\mathbf{l} V_{\mathbf{k}-\mathbf{l}}\left[f^e_\mathbf{l} + f^h_{\mathbf{l}-\mathbf{q}}\right], \quad (76)$$

and the stimulated contribution

$$\Omega_{\rm ST}(\mathbf{k}; q_z\mathbf{q}) \equiv \sum_{q'_z} i\mathcal{F}_{\mathbf{q},q'_z}\Delta\langle B^\dagger_{q_z,\mathbf{q}} B_{q'_z,\mathbf{q}}\rangle + \sum_\mathbf{l} V_{\mathbf{k}-\mathbf{l}}\Delta\langle B^\dagger_{q_z,\mathbf{q}} a^\dagger_{v,\mathbf{l}} a_{c,\mathbf{l}-\mathbf{q}}\rangle. \quad (77)$$

The coupling to coherent correlations and correlated triplets is described schematically by $D^{coh}_{\mathbf{k},\mathbf{q}}$ and $T_{\mathbf{k},\mathbf{q}}$, respectively. In general, equations (74) and (75) constitute *the semiconductor luminescence equations*. The first line of equation (75) resembles the semiconductor Bloch equations; renormalized kinetic energies $\tilde\epsilon$ and phase-space filling, $1 - f^e - f^h$, can be identified directly [1]. The second line introduces a new source term: as long as there is a carrier density excited in the system, the singlet contribution $f^e f^h$ drives photon-assisted recombinations leading to a build-up of photon numbers even if the coherence and correlation contributions vanish initially. As a result, $\Delta\langle B^\dagger a^\dagger_v a_c\rangle$ is generated, i.e., $f^e f^h$ provides a spontaneous

emission source to the recombination process. According to the factor $f^e_{\mathbf{k}} f^h_{\mathbf{k}-\mathbf{q}}$, the spontaneous emission takes place only if an electron at $\mathbf{k}$ and a hole at $\mathbf{k}-\mathbf{q}$ are present simultaneously. The spontaneous emission source is modified by the correlated part, $\Delta\langle a^\dagger_c a^\dagger_v a_c a_v\rangle$, which includes the possibility to emit light directly from true exciton populations. As the photoluminescence starts to build up, the stimulated contribution $\Omega^{\rm inc}_{ST}$ can alter the emission spectrum. To obtain a closed set of equation, one also has to solve simultaneously the dynamics of the carrier densities, $\Delta\langle a^\dagger_c a^\dagger_v a_c a_v\rangle$, $\Delta\langle a^\dagger_c a^\dagger_c a_c a_c\rangle$, $\Delta\langle a^\dagger_v a^\dagger_v a_v a_v\rangle$, and the phonon terms.

5.1 Radiative decay

The spontaneous recombination adds a new term to the density and exciton-correlation equations. The incoherent source terms for the carrier distributions and the excitonic correlations are

$$\hbar\frac{\partial}{\partial t} f^e_{\mathbf{k}}|_{\rm SE} = -\,2{\rm Re}\left[\sum_{\mathbf{q},q_z} \mathcal{F}_{\mathbf{q},q_z}\Delta\langle B^\dagger_{\mathbf{q}}\, a^\dagger_{v,\mathbf{k}-\mathbf{q}} a_{c,\mathbf{k}}\rangle\right], \quad (78)$$

$$\frac{\partial}{\partial t} f^h_{\mathbf{k}}|_{\rm SE} = -\,2{\rm Re}\left[\sum_{\mathbf{q},q_z} \mathcal{F}_{\mathbf{q},q_z}\Delta\langle B^\dagger_{\mathbf{q}} a^\dagger_{v,\mathbf{k}} a_{c,\mathbf{k}+\mathbf{q}}\rangle\right], \quad (79)$$

$$\begin{aligned} i\hbar\frac{\partial}{\partial t} c^{\mathbf{q},\mathbf{k}',\mathbf{k}}_{\rm X}|_{\rm SE} = \\ -i\left(1-f^e_{\mathbf{k}}-f^h_{\mathbf{k}-\mathbf{q}}-\right)\sum_{q_z}\mathcal{F}_{\mathbf{q},q_z}\Delta\langle B^\dagger_{\mathbf{q},q_z} a^\dagger_{v,\mathbf{k}'} a_{c,\mathbf{k}'+\mathbf{q}}\rangle \\ -i\left(1-f^e_{\mathbf{k}'-\mathbf{q}}-f^h_{\mathbf{k}'}\right)\sum_{q_z}\mathcal{F}_{\mathbf{q},q_z}\Delta\langle B_{\mathbf{q},q_z} a^\dagger_{c,\mathbf{k}} a_{v,\mathbf{k}-\mathbf{q}}\rangle, \end{aligned} \quad (80)$$

respectively. As a distinct difference between the carrier and exciton recombination, we notice that all momentum states $\mathbf{k}$ of $f^{e(h)}_{\mathbf{k}}$ can recombine radiatively, whereas the exciton populations couple to the light field only if their center-of-mass momentum matches with the in-plane momentum, $\mathbf{q}$, of the photons.

To analyze the effect of spontaneous emission on exciton and carrier distributions, we plot them at different time moments after the same $1s$ excitation used in Figure 6. We observe that carrier densities are quickly generated and, after that, they do not show much evolution since the total radiative loss rate is rather slow. The $1s$-excitons are clearly generated with a wide spread of momentum since for the chosen excitation condition, the conversion is dominated by phonon scattering [25] which does not have a strong momentum selectivity. After and during the conversion, we observe that the very low momentum excitons, roughly those with $|\mathbf{q}|a_0 < 0.1$, show a fast decay due to photoluminescence related recombination. The excitons in these momentum states are optically active, i.e. these are the 'bright excitons' that give rise to luminescence. Due to its momentum selectivity this recombination leads to a significant hole burning in the exciton distributions [5]. Since the typical radiative decay time for these bright excitons is on the order of of 10 ps [26–28],

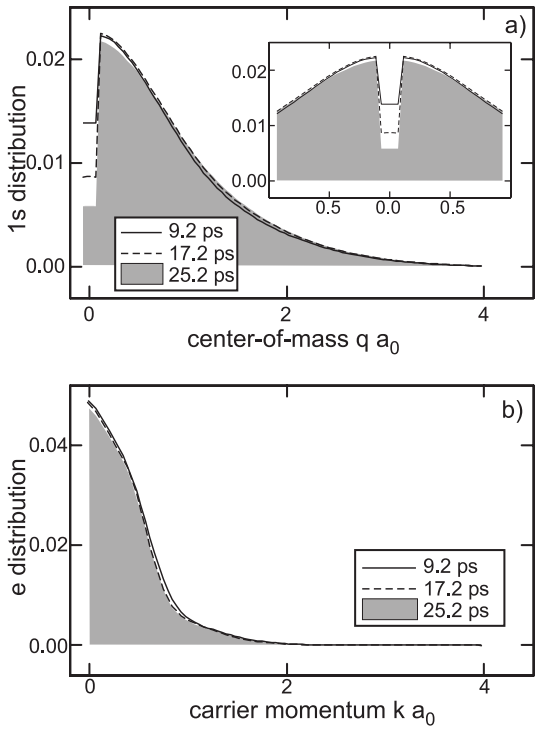

Fig. 6. (a) Computed $1s$-exciton and (b) carrier distributions for a time sequence after the resonant $1s$ excitation described in Figure 2. The inset shows the excitonic center-of-mass distribution in the vicinity of the optically active low-momentum states.

the majority of all the excitons is predominantly in 'dark states'.

Since an electron with any momentum $\mathbf{k}$ can recombine with a hole having a corresponding momentum, electron and hole distributions do not show a momentum selectivity such that they change slowly on a nanosecond time scale. This critical difference between exciton and carrier distributions makes excitons highly nonthermal even if carriers are in a thermal quasi equilibrium. This fundamental characteristics can be seen as nonequilibrium features in exciton photoluminescence [23,28,29]. The related luminescence spectra

$$I_{\rm PL}(\omega_{\mathbf{q}}) = \frac{\partial}{\partial t}\Delta\langle B^\dagger_{\mathbf{q},q_z} B_{\mathbf{q},q_z}\rangle, \quad (81)$$

which is strictly valid for steady state emission [13], are shown in Figure 7 for matching times and excitation of Figure 6. We observe that the luminescence follows the hole-burning dynamics and that the $1s$ resonance remains in the spectrum even when the optically active excitons are significantly decayed.

5.2 Analytic luminescence formula

In order to gain some further insights into the spectral features and the population dependence of the semiconductor

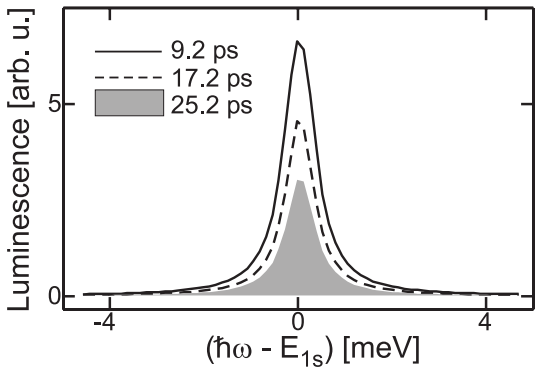

Fig. 7. Photoluminescence spectra computed for different times after the 1s excitation presented in Figure 2. The time moments are identical to those used for Figure 6.

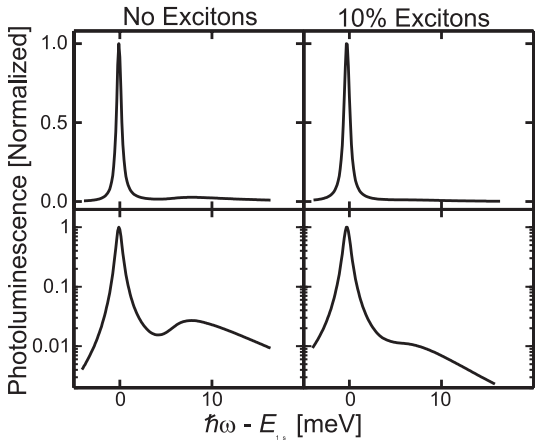

Fig. 8. Comparison of computed luminescence spectra on a linear (top figures) and a logarithmic scale (bottom figures). The figures on the left-hand side show the results for the quasi-equilibrium electron-hole luminescence at a temperature of 77 K without any excitonic populations and the figures on the right-hand side include 10% excitons in a thermal distribution. The spectra have been computed for a carrier density of $10^{10}\,\mathrm{cm}^{-2}$.

luminescence, we look for an analytic solution under incoherent conditions. In many experimentally relevant situations, the carrier system changes slowly such that the populations f^{λ} and $\Delta\langle a_c^\dagger a_v^\dagger a_c a_v\rangle$ can be taken as constant. For such situations, the incoherent equations (74) and (75) are closed. We furthermore replace the specific form of triplet scattering by a constant dephasing. If we generalize the analytical correlation (58) to allow for exciton populations, we find

$$\Delta\langle X^\dagger_{\lambda,\mathbf{q}} X_{\nu,\mathbf{q}}\rangle = \Delta N_\lambda(\mathbf{q})\delta_{\lambda,\nu} - \frac{E_\nu - E_\lambda}{E_\nu - E_\lambda - i\gamma}\langle X^\dagger_{\lambda,\mathbf{q}} X_{\nu,\mathbf{q}}\rangle_{\mathrm{S}}, \quad (82)$$

where $\Delta N_\lambda(\mathbf{q})$ determines the population of excitons in state λ while the remaining term is the correlated part of the electron-hole plasma. For small enough γ, equation (82) reduces to

$$\Delta\langle X^\dagger_{\lambda,\mathbf{q}} X_{\nu,\mathbf{q}}\rangle = \Delta N_\lambda(\mathbf{q})\delta_{\lambda,\nu} - (1-\delta_{\lambda,\nu})\,\langle X^\dagger_{\lambda,\mathbf{q}} X_{\nu,\mathbf{q}}\rangle_{\mathrm{S}}, \quad (83)$$

which we will use in the further analysis.

Within this approximation scheme, we obtain a simple expression for the photoluminescence spectrum which is given as the steady-state photon flux,

$$I_{\mathrm{PL}}(\omega_\mathbf{q}) = \frac{2|\mathcal{F}_\mathbf{q}|^2}{\hbar} \times \mathrm{Im}\left[\sum_\lambda \frac{|\phi^R_\lambda(r=0)|^2\left[\Delta N_\lambda(\mathbf{q}) + \langle X^\dagger_{\lambda,\mathbf{q}} X_{\lambda,\mathbf{q}}\rangle_{\mathrm{S}}\right]}{E_\lambda - \hbar\omega_q - i\gamma}\right]. \quad (84)$$

As mentioned above, this result is valid only for low densities and negligible broadening. However, the extension for higher densities is straight forward in the same way as for the Elliot formula (51). Consequently, we find similar density-dependent features, such as frequency and exciton-index dependent renormalizations of ϕ_ν, E_ν, and γ [23].

Comparing equations (84) and (51) we note strong similarities. In particular, the frequency dependence of both equations is governed by the same denominator giving rise to excitonic resonances. Hence, we can already conclude at this point, that the appearance of these resonances is independent of the detailed structure of the factor appearing in the numerator of equation (84). In particular, the singlet term,

$$\langle X^\dagger_{\lambda,\mathbf{q}} X_{\lambda,\mathbf{q}}\rangle_{\mathrm{S}} = \sum_{\mathbf{k}} \phi^L_\lambda(\mathbf{k}) f^e_{\mathbf{k}+\mathbf{q}_e} f^h_{\mathbf{k}-\mathbf{q}_h} \phi^L_\lambda(\mathbf{k}), \quad (85)$$

describes excitonic photoluminescence from correlated electron-hole plasma populations while $\Delta N_\lambda(\mathbf{q})$ corresponds to the true exciton population luminescence. Since the electron-hole plasma and exciton population terms appear additively in ΔN_λ, both contributions can lead to luminescence and therefore also to emission at the excitonic resonances. Thus, the mere appearance of luminescence, e.g., at the 1s-resonance cannot be taken as a unique signature of exciton populations [3].

To illustrate these features, we show in Figure 8 normalized luminescence spectra that have been computed with (right column) and without (left column) an incoherent excitonic population in a quantum-well system. First of all, we note that the spectra are dominated by a strong 1s-resonance in both cases. Whereas it is basically impossible to identify exciton population effects in the normalized spectra on a linear scale (top figures), we see that the logarithmic scale (bottom figures) reveals a characteristic difference in the ratio of the 1s and 2s or bandedge luminescence. A quantitative analysis of this ratio in a series of experimental measurements for different excitation conditions makes it possible to extract informations about the excitonic population of the optically active states [23]. However, the total exciton population is not directly accessible via PL experiments.

6 Terahertz spectroscopy

An unambiguous method to identify excitonic populations is to perform terahertz (THz) spectroscopy, i.e. to probe transitions between excitonic eigenstates [4,5]. Under incoherent conditions, the observation of resonances due to these transitions is a clear signature of an exciton population.

For the theoretical description of THz processes, the light-matter interaction discussed in this article has to be extended to include the coupling to intraband quantities. Microscopically, this interaction follows from

$$H_{\mathrm{THz}} = -A(t)\sum_{k}\left[j_c(\mathbf{k})a^{\dagger}_{c,\mathbf{k}}a_{c,\mathbf{k}} + j_v(\mathbf{k})a^{\dagger}_{v,\mathbf{k}}a_{v,\mathbf{k}}\right] + \frac{Q^2A^2(t)}{2m_0}\sum_{k}\left[a^{\dagger}_{c,\mathbf{k}}a_{c,\mathbf{k}} + a^{\dagger}_{v,\mathbf{k}}a_{v,\mathbf{k}}\right], \quad (86)$$

which includes the current-matrix element

$$j_\lambda(\mathbf{k}) \equiv \frac{Q\hbar\mathbf{k}\cdot\mathbf{e}_\sigma}{m_\lambda}, \quad (87)$$

with the effective mass m_λ and polarization direction of the field $\mathbf{e}_\sigma$ which lies in the QW plane. The derivation providing j_λ with an effective mass is performed, e.g., in reference [30].

In general, the A^2 term only leads to refractive index changes and it is largely suppressed in Coulomb-interacting systems [30], such that the THz absorption follows entirely from the macroscopic current

$$J \equiv \sum_{k}\left[j_e(\mathbf{k})f^e_{\mathbf{k}} + j_h(\mathbf{k})f^h_{\mathbf{k}}\right]. \quad (88)$$

The relation between the many-body states and the THz response becomes clearest when we focus on the situation where all interband coherences vanish (i.e., $\mathbf{P} = 0$) and $\mathbf{A}$ is in the THz regime. Under these conditions, only the excitonic correlations couple directly to THz field, which makes *THz absorption uniquely qualified method to directly detect many-body correlations under incoherent conditions*. In practice, we need to solve the following incoherent equations

$$J_{\mathrm{THz}} = \frac{1}{\mathcal{S}}\sum_{\mathbf{k},\lambda} j_\lambda(\mathbf{k})f^\lambda_{\mathbf{k}}, \quad (89)$$

$$\frac{\partial}{\partial t}f^e_{\mathbf{k}} = -\frac{2}{\hbar}\mathrm{Im}\left[\sum_{\mathbf{q},\mathbf{k}'} V_{\mathbf{k}'+\mathbf{q}-\mathbf{k}}c_{\mathrm{X}}^{\mathbf{q},\mathbf{k}',\mathbf{k}} - \sum_{\mathbf{q},\mathbf{k}'} V_{\mathbf{q}}c_{c,c,c,c}^{\mathbf{q},\mathbf{k}',\mathbf{k}}\right], \quad (90)$$

$$\frac{\partial}{\partial t}f^h_{\mathbf{k}} = +\frac{2}{\hbar}\mathrm{Im}\left[\sum_{\mathbf{q},\mathbf{k}'} V_{\mathbf{k}'-\mathbf{q}-\mathbf{k}}c_{\mathrm{X}}^{\mathbf{q},\mathbf{k},\mathbf{k}'} - \sum_{\mathbf{q},\mathbf{k}'} V_{\mathbf{q}}c_{v,v,v,v}^{\mathbf{q},\mathbf{k}',\mathbf{k}}\right], \quad (91)$$

$$i\hbar\frac{\partial}{\partial t}c_{\mathrm{X}}^{\mathbf{q},\mathbf{k}',\mathbf{k}}|_{\mathrm{THz}} = +j(\mathbf{k}'+\mathbf{q}-\mathbf{k})A(0,t)c_{\mathrm{X}}^{\mathbf{q},\mathbf{k}',\mathbf{k}}, \quad (92)$$

where only the THz part is expressed for $c_{\mathrm{X}}^{\mathbf{q},\mathbf{k}',\mathbf{k}}$; the other parts can be found in equation (52).

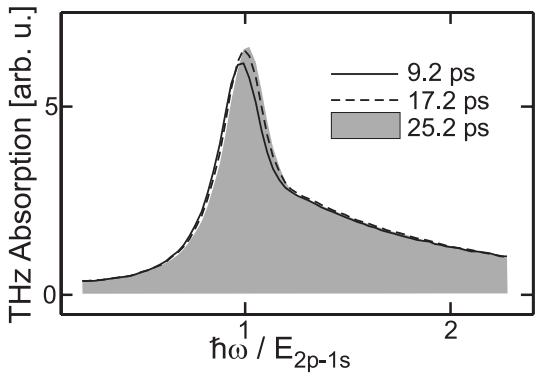

Fig. 9. Terahertz spectra determined at different time moments after the resonant $1s$ excitation used in Figure 2. The time sequence is identical to that of Figure 6.

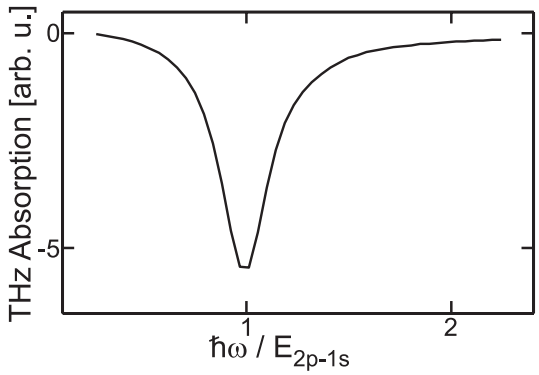

Fig. 10. Computed THz spectrum at the final time after resonant $2s$ excitation as shown in Figure 3. The negative absorption indicates optical gain in the THz regime.

To illustrate the basic capabilities of THz spectroscopy, we evaluate the THz absorption for the same computation as in Figure 6 following a resonant $1s$ excitation. We observe that a clear $1s$ to $2p$ transition resonance can be seen, verifying the presence of $1s$ populations. We also observe that the hole burning of optically active excitons has only a small effect of the THz absorption, showing that this spectroscopy is sensitive to both bright and dark exciton populations.

In the case of the resonant $2s$ excitation, one could reach a situation where one has a population inversion between the $1s$ and $2p$ states. Under such conditions, the THz response shows clear gain signatures, as can be seen in Figure 10, where we plot the THz response for the final time of $2s$ excitation analyzed in Figure 3.

In order to obtain some analytic insights, we now make adiabatic approximations which can be applied when those parts of $f^{e(h)}$ and c_{X} that are independent of the THz field have a slow temporal variation. Under these conditions, the exciton correlation dynamics (56) can be

generalized to include the THz excitation

$$i\hbar\frac{\partial}{\partial t}\Delta\langle X^{\dagger}_{\lambda,\mathbf{q}}X_{\nu,\mathbf{q}}\rangle = (E_\nu - E_\lambda)\,\Delta\langle X^{\dagger}_{\lambda,\mathbf{q}}X_{\nu,\mathbf{q}}\rangle - (E_\nu - E_\lambda)\,\langle X^{\dagger}_{\lambda,\mathbf{q}}X_{\nu,\mathbf{q}}\rangle_{\mathrm{S}} + \sum_\beta [J_{\lambda,\beta}\Delta\langle X^{\dagger}_{\beta,\mathbf{q}}X_{\nu,\mathbf{q}}\rangle - J_{\nu,\beta}\Delta\langle X^{\dagger}_{\lambda,\mathbf{q}}X_{\beta,\mathbf{q}}\rangle]A(t) + T^{\lambda,\nu}(\mathbf{q}), \tag{93}$$

where we have defined the THz transition matrix element

$$J_{\nu,\lambda} = \sum_{\mathbf{k}} \phi^{\star}_{\nu}(\mathbf{k})j(\mathbf{k})\phi_\lambda(\mathbf{k}). \tag{94}$$

This expression implies the typical dipole selection rules, i.e. J is vanishing for $\nu = \lambda$, whereas e.g. $\nu = 1s$ and $\lambda = 2p$ gives non-zero contributions.

If we assume that $c^{\mathbf{q},\mathbf{k}',\mathbf{k}}_{c,c}$ leads to a simple decay of THz currents and replace the triplet term by a phenomenological dephasing, we can write the analytic solution for the linear THz susceptibility

$$\chi_{\mathrm{THz}}(\omega) = -\frac{1}{\epsilon_0\hbar\omega^2(\omega + i\Gamma)}\sum_{\nu,\lambda}\left(S^{\nu,\lambda}_{\omega}\Delta n_{\nu,\lambda} - \left[S^{\nu,\lambda}_{-\omega}\Delta n_{\nu,\lambda}\right]^{\star}\right). \tag{95}$$

This solution involves the response function

$$S^{\nu,\lambda}_{\omega} = \sum_\beta \frac{(E_\nu - E_\beta)\,J_{\nu,\beta}J_{\beta,\lambda}}{E_\beta - E_\nu - \hbar\omega - i\gamma}. \tag{96}$$

In the case that only exciton populations exist, i.e. $\Delta n_{\nu,\lambda} = \delta_{\nu,\lambda}\Delta n_{\nu,\nu} \equiv \delta_{\nu,\lambda}\Delta n_\nu$, equation (95) reduces to

$$\chi_{\mathrm{atom}}(\omega) = -\frac{1}{\epsilon_0}\sum_\nu \left(S^{\nu}_{\mathrm{atom}}(\omega) - [S^{\nu}_{\mathrm{atom}}(-\omega)]^{\star}\right)\Delta n_\nu, \tag{97}$$

$$S^{\nu}_{\mathrm{atom}}(\omega) = \sum_\beta \frac{|D_{\nu,\beta}|^2}{E_\beta - E_\nu - \hbar\omega - i\gamma}, \tag{98}$$

where $D_{\nu,\lambda} = \langle\phi_\nu|e\mathbf{r}\cdot\mathbf{e}_P|\phi_\lambda\rangle$ defines the excitonic dipole-matrix element. Equation (98) has a form that is typical for an atomic absorption spectrum when different atomic levels are populated according to Δn_ν. Consequently, the correlation Δn_ν has a one-to-one correspondence to the atom number in state ν. This identification supports the concept of exciton populations and the separation of population and correlated plasma contributions to the luminescence, as used in the analytic luminescence formula (84).

7 Summary

The examples in this paper demonstrate the current status of the systematic many-body approach to describe the semiclassical and quantum-optical properties of semiconductor structures. The cluster-expansion of the relevant correlation functions is a viable procedure to construct closed sets of equations at well defined levels of approximation. For special situations, these equations can be solved analytically, allowing us to gain important insights into the basics of light-matter interaction. Besides the Elliot formula for the semiclassical absorption coefficient, which has been known since many decades, we derive a similar equation for the light emission. As for the absorption, also the emission resonances are determined by the characteristic eigenergies of the Coulomb interacting system, i.e., by the exciton resonances. Hence, for conditions where these resonances are present, i.e. at not too high temperatures and densities, they will dominate the emission spectra. As a consequence, the luminescence is centered around the $1s$-exciton resonance, even if the electron-hole system exists in the form of plasma populations without true excitons.

Under suitable conditions, the theory predicts the presence of incoherent excitonic populations in the system. Most properties of these excitons are strongly influenced by the fermionic structure of the constituent quasiparticles. Excitonic populations efficiently contribute to the luminescence as long as the optically active, energetically low momentum states are occupied. Consequently, the radiative decay leads to hole burning in the excitonic distribution, leaving most of the excitonic populations in dark states. The calculations show that the presence of excitonic populations in bright and dark states leads to characteristic signatures in the induced absorption of a THz probe field, which measures the transitions between the excited quasiparticle states.

For resonant excitation, it is shown that the coherent optical polarization can be efficiently converted into $1s$-exciton populations for sufficiently low excitation level. If the excitation is tuned to the $2s$-resonance a mixture of excitons in $2s$- and $2p$-states is generated leading to a population inversion between the $2p$- and $1s$-states which manifests itself in gain for a THz probe field.

This work was supported by the Optodynamics Center and the Deutsche Forschungsgemeinschaft through the Quantum Optics in Semiconductors Research Group.

References

1. H. Haug, S.W. Koch, *Quantum Theory of the Optical and Electronic Properties of Semiconductors*, 4th edn. (World Scientific Publ., Singapore, 2004)
2. Several articles in *Semiconductor Optics*, edited by H. Kalt (Springer, Berlin, 2004)
3. M. Kira, F. Jahnke, S.W. Koch, Phys. Rev. Lett. **81**, 3263 (1998)
4. R. Groeneveld, D. Grischkowsky, J. Opt. Soc. Am. B **11**, 2502 (1994)
5. M. Kira, W. Hoyer, T. Stroucken, S.W. Koch, Phys. Rev. Lett. **87**, 176401 (2001)

6. J. Cerne et al., Phys. Rev. Lett. **77**, 1131 (1996)
7. R. Kaindl, M.A. Carnahan, D. Hägele, D.S. Chemla, Nature **423**, 734 (2003)
8. M.C. Beard, G.M. Turner, C.A. Schmuttenmaer, Phys. Rev. B **62**, 15764 (2000)
9. R. Huber et al., Nature **414**, 286 (2001)
10. S. Hughes, D. Citrin, J. Opt. Soc. Am. B **17**, 128 (2000)
11. T. Meier, G. von Plessen, P. Thomas, S.W. Koch, Phys. Rev. Lett. **73**, 902 (1994)
12. C. Cohen-Tannoudji, J. Dupont-Roc, G. Grynberg, *Photons & Atoms* (Wiley, New York, 1989)
13. M. Kira, F. Jahnke, W. Hoyer, S.W. Koch, Prog. Quant. Electr. **23**, 189 (1999)
14. F. Jahnke, M. Kira, S.W. Koch, Z. Phys. B **104**, 559 (1997)
15. A. Thränhardt, S. Kuckenburg, A. Knorr, T. Meier, S.W. Koch, Phys. Rev. B **62**, 2706 (2000)
16. H.W. Wyld, B.D. Fried, Ann. Phys. **23**, 374 (1963)
17. J. Fricke, Ann. Phys. **252**, 479 (1996)
18. W. Hoyer, M. Kira, S.W. Koch, Phys. Rev. B **67**, 155113 (2003)
19. D.F. Walls, G.J. Milburn, *Quantum Optics*, 1st edn. (Springer-Verlag, New York, 1994)
20. T. Usui, Prog. Theor. Phys. **23**, 787 (1960)
21. R. Elliot, in *Polarons and Excitons*, edited by C. Kuper, G. Whitefield (Oliver and Boyd, Boston, 1963), p. 269
22. F. Jahnke et al., Phys. Rev. Lett. **77**, 5257 (1996)
23. S. Chatterjee et al., Phys. Rev. Lett. **92**, 067402 (2004)
24. S.W. Koch, M. Kira, W. Hoyer, V. Filinov, Phys. Stat. Sol. (b) **238**, 404 (2003)
25. M. Kira, S.W. Koch, Phys. Rev. Lett. **93**, 076402 (2004)
26. G. Khitrova, H. M. Gibbs, F. Jahnke, M. Kira, S. W. Koch, Rev. Mod. Phys. **71**, 1591 (1999)
27. V. Agranovich, O. Dubowskii, JETP Lett. **3**, 223 (1966).
28. Szczytko et al., Phys. Rev. Lett. **93**, 137401 (2004)
29. R.F. Schnabel et al., Phys. Rev. B **46**, 9873 (1992)
30. M. Kira, W. Hoyer, S.W. Koch, Phys. Stat. Sol. (b) **238**, 443 (2003)